TRANSFORMATION AND MICROSTRUCTURE EVOLUTION DURING THERMOMECHANICAL PROCESSING

An Investigation of Energy Dissipation in Beta III Titanium Alloy

JACOPO ROMANÒ [1,3] SIMONE DI GIUSEPPE,[1] FABIO LAZZARI [1]
LORENZO GARAVAGLIA [1] FRANCESCO VOLONTE' [1,2] and
SIMONE PITTACCIO [1]

01.—Institute of Condensed Matter Physics and Technologies for Energy (CNR-ICMATE), National Research Council of Italy, Via Previati 1/E, Lecco, Italy. 02.—Department of Chemistry, Materials and Industrial Chemistry (CMIC), Politecnico di Milano, Piazza Leonardo da Vinci, 32, Milan, Italy. 3.–e-mail: jacopo.romano@icmate.cnr.it

This work investigates the effects of a supertransus annealing treatment, followed by plastic deformation, on the damping properties of a Ti-11.5Mo-6Zr-4.5Sn alloy. In our study, no evidence of α″-phase was found. A heat treatment at 800°C for 180 min, followed by 16% tensile plastic deformation, successfully increased the energy dissipation of the alloy, with an increase up to 76% in quasi-static hysteresis, and up to 200% in dynamic damping factor. The results of metallographic analysis, mechanical tests, and X-ray powder diffraction suggest that this increase in damping capacity may be caused by reversible twinning, and not necessarily by stress-induced α″ martensite.

INTRODUCTION

Titanium alloys are a class of metallic materials, which is particularly exploited for its good mixture of structural and corrosion- and heat-resistant properties, coupled with low density.[1] In particular, the metastable beta (β) alloys, obtained by the addition of sufficient amounts of β-stabilizing elements (Mo, Cr, V, Fe, …), are especially interesting for their good formability in the solution-treated condition and their excellent hardenability, compared to the alpha (α) or alpha/beta (α/β) alloys. High strengths can be achieved in the metastable β-alloys by aging treatments directed to the precipitation of a finely dispersed α-phase. Due to these characteristics, β-Ti alloys have attracted much attention for aerospace[2] and biomedical[3] applications, where they may be preferred to the widespread α/β alloys, chiefly in consideration of their higher yield strengths or lower Young's moduli. Another interesting feature displayed by some compositions in this group is their pseudo-elasticity,[4] which makes them possible alternatives to intermetallic NiTi shape memory alloys. Pseudo-elasticity, a property tightly linked to the activation of stress-induced martensitic transformations, provides high deformability, and occurs in conjunction to a rather large hysteresis[5] and corresponding energy loss coefficients.

The combined optimization of strength and damping capacity could be of interest for structural applications, where intensely loaded elements are subjected to vibration, impulsive, or dynamic forces in general, e.g., in the aerospace field. To the best of our knowledge, there are very limited reports[6,7] of research in that sense.

The main mechanisms producing damping in β-Ti alloys are of the Snoek type (e.g. involving interstitial oxygen, as in Ti-Nb-O alloys;[8,9] the stress-induced movements of defects such as dislocations or boundaries (grain boundaries, twin boundaries, domain boundaries, and the boundaries between martensite variants),[10] or a stress-induced martensitic (SIM) phase transformation. The addition of oxygen can initially produce strengthening as well as damping, and thus could be of interest, but, unfortunately, increasing the concentration of interstitials in order to maximize damping may lead to brittle behavior.[9] The phenomena involving microstructural characteristics and their relationship with deformation mechanisms may offer useful opportunities.

The deformation mechanisms of β-Ti alloys have been described by several groups,[4,11–13] and it has been demonstrated that different mechanisms predominate, depending on chemical factors. That

effect of chemistry can be summarized using indices like the molybdenum equivalent of the alloy ([Mo]-eq), or, much more precisely, by combining measures such as the mean d-orbital energy level, $\overline{M_d}$, and the mean bond order $\overline{B_o}$ into a $\overline{B_o}$ versus $\overline{M_d}$ map (or Kuroda map).[11] According to the latter model, the metastable β-alloys with high $\overline{B_o}$ and low $\overline{M_d}$ tend to slip, those with intermediate values of both parameters form twins, and there is a group of compositions with $\overline{M_d}$ higher values (neighboring the α/β range), which can undergo martensitic transformations. Yet another method proposed by Bignon et al.[12] can be used to describe these variations: it is based on an empirical Fe-equivalent (iron-equivalent), and the martensitic start temperature, M_s. As specified by that criterion, besides a slip/twin region for higher values of the Fe-equivalent, there is a superelastic range corresponding to low Fe-equivalent and intermediate M_s (from −90°C to 90°C), and a TRIP (transformation-induced plasticity) regime for low Fe-equivalent and higher M_s values.

In this study, we consider Beta III titanium alloy (Ti-11.5Mo-6Zr-4.5Sn), a metastable β-alloy with high strength, good hardenability, good resistance to stress corrosion, and good cold-formability that has already found application in the aerospace field, especially for aircraft fasteners and sheet metal parts. This alloy is peculiar, because it displays high mechanical properties, especially in the aged condition, and has a special positioning in both the Kuroda and the M_s versus Fe-equivalent maps. According to both, slip and twinning are the main mechanisms associated with the Beta III alloy, in the two diagrams, this composition is positioned very close to the boundary separating the twinning/slip field from the martensitic and TRIP region, respectively. Indeed, some studies in the literature investigated the correlation between microstructure and pseudo-elastic properties of the Beta III titanium alloy. Laheurte et al.[14,15] explored two different annealing treatments (800°C and 900°C for up to 2 h) and the application of loading/unloading cycles with increasing imposed strain up to 20%. They established that temperature, strain, and grain size affect the deformation behavior. In particular, they reported that thermos-elastic martensite (α"-phase) could be identified in the material with heat treatment at 800°C (e.g., for 1 h, final grain size 53 μm) followed by plastic deformation. The largest hysteresis was obtained after plastic deformation to 12%. Also, martensite was observed only for a minimum grain size of 23 μm. Cai et al.[16,17] heated a cold-drawn wire for 1.5 min at different temperatures (from 816°C to 1093°C) and quenched it. The mechanical strength of the samples decreased with increasing grain size (the maximum size was 85 μm when treated at 1093°C). Micrographs showed that, after the annealing treatment, the material consisted of single β-phase. After a plastic deformation of 16%, however, striations were observed, that are

reported by authors to be evidence of either twinning or stress-induced martensite. The presence of SIM in the deformed sample was confirmed by the identification of two X-ray peaks compatible with α" after cold working.

Here, we present a study of the damping properties of the Beta III titanium alloy in relationship to microstructural modifications. In particular, we investigate the effects of annealing treatments followed by plastic deformation, and monitor the microstructural changes through X-ray diffraction and optical and electron microscopy. The damping behavior of the material in terms of hysteresis and internal friction response has been evaluated through quasi-static tensile tests and dynamic mechanical analysis (DMA). Our present findings support the idea that non-martensitic phenomena could play a role in the development of the observed trends.

MATERIALS AND METHODS

Material: Beta III Titanium

Beta III titanium alloy wire with a diameter of 2 mm was provided by Perryman (Houston, PA, USA) in a solution-annealed supply state. Energy dispersive X-ray spectroscopy (EDX; Oxford Instruments, High Wycombe, UK) provided a composition (Mo 11.19 wt.%, Zr 6.08 wt.%, Sn 4.69 wt.%, Ti balance) for the as-received material, which lies well within the reference range for Beta III.[18] The composition of our batch corresponds to a [Mo]-eq of 8.61% (cf. [Mo]-eq=9.00% for the standard alloy Ti-11.5Mo-6Zr-4.5Sn). The Kuroda map parameters calculated for our batch composition were $\overline{B_o}$= 2.8070 and $\overline{M_d}$ = 2.4265, versus $\overline{B_o}$= 2.8078 and $\overline{M_d}$ = 2.4257 for the standard alloy.

As highlighted by thermogravimetric and differential thermal analysis (TG-DTA) using a Q600 SDT (TA Instruments; New Castle, DE, USA), the microstructure of the as-received sample (Fig. 1) was largely characterized by β-grains, which are
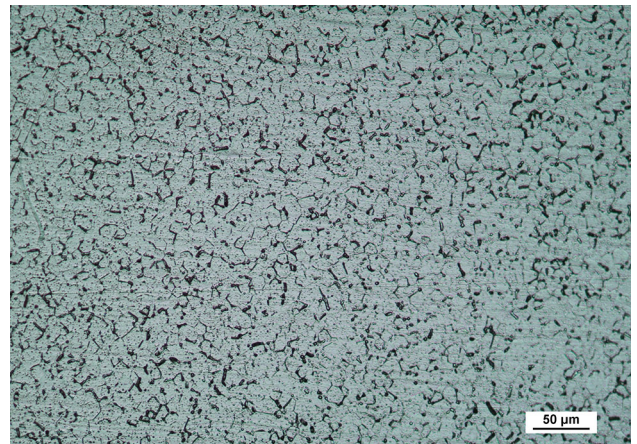

Fig. 1. Microstructure of the as-received sample; etched with an oxalic tint

partially transformed into ω- and α-phases between approximately 350°C and 400°C and between 400°C and 700°C, respectively, as witnessed by the endothermic down-pointing peaks. The reverse transformation occurs upon reaching the beta-transus temperature at ca. 780°C and ends at 842°C. No clear transformation peaks were detected during cooling. All these temperatures are consistent with literature data.[19]

Thermomechanical Treatments

Samples (12 cm) were cut from the material in as-received conditions, which were exposed to the different heat treatments summarized in Table I, followed by quenching in water.

Note that, for Beta III, the beta-transus T_β is at 780°C. Furthermore, AG is the standard treatment for peak aging (subcritical annealing and isothermal precipitation of the α-phase). The treatment selected by Laheurte et al.[15] to induce SIM (R800-60m) was taken as a reference for comparison. Similar treatments with extended durations (N800-90m, and N800-180m) were tested as novel proposed processes.

Besides heat treatment, the samples were also subjected to tensile deformation (none, 9%, 12%, and 16%) prior to further testing. A post-deformation fast-annealing treatment (P470-5m) was tried, and the short duration and the temperature were chosen in order to avoid phase transformations from the β-phase.[18]

Metallography

Metallographic specimens were prepared by mounting a few segments of each heat-treated and deformed wire sample in epoxy resin. After planar-grinding (to 4000 grit) and polishing (to 1 μm), the specimens were observed as-polished and after etching with either Kroll's reagent ($H_2O + HNO_3 + HF$, 92:6:3 vol.%), or a mixture of saturated oxalic acid solution and HF (98:2 vol.%), later diluted 1:5 in water, to slow the reaction with the sample.

Light microscopy was carried out using a Leitz-Aristomet microscope (Wetzlar, Germany) in bright-field and cross-polarized conditions. Average grain size was evaluated from the bright-field images of the specimens (exposed to Kroll's reagent to highlight the grain boundaries) by counting border intercepts with straight lines of known length. Scanning electron microscopy (SEM) was carried out using a Leo 1430 (Carl Zeiss, Oberkochen, Germany) with secondary electron and backscattered electron contrasts. Microanalysis was obtained by EDX (Oxford Instruments).

Quasi-Static Mechanical Characterization

The tensile mechanical response was evaluated through cyclic loading at incrementally larger maximal strains (0.2%, 0.3%, 0.4%, 0.5%, 1%, 1.5%, 2%, 2.5%, 3%, 3.5%, and 4%) using an ElectroPuls E3000 (Instron, High Wycombe, UK). Besides the Young's modulus and yield point, the hysteresis areas of the cycles were calculated as a measure of damping (energy dissipation).

Dynamic Mechanical Analysis (DMA)

Samples were pre-strained of 0.5% and then subjected to a sinusoidal load at increasing frequency from 0.1 Hz to 20 Hz (0.1 Hz, 0.25 Hz, 0.5 Hz, 0.75 Hz, 1 Hz, 2.5 Hz, 5 Hz, 7.5 Hz, 10 Hz, 12.5 Hz, 15 Hz, 17.5 Hz, and 20 Hz). The number of cycles for the different frequencies was selected in order to reach steady state (constant amplitudes). The frequency sweep was repeated for different strain amplitudes (0.2%, 0.3%, 0.4%, 0.5%, 1%, 1.5%, 2%, 2.5%, 3%, and 3.5%). Tests were carried out using the ElectroPuls E3000. In order to assess the visco-elastic properties of the material, storage and loss moduli were calculated, as well as tanδ, which was taken as a measure of damping capacity.

X-Ray Powder Diffraction

X-ray diffraction (XRD) experiments were conducted using an X'Pert Pro MPD X-ray diffractometer (PANalytical; Almelo, Netherlands)

Table I. Sample name, with temperature, duration, type, and atmosphere of the heat treatments

Sample	Temperature (°C)	Duration	Atmosphere	Type
AR	–	–	–	Quality check
SA	700	1 h	Ar	Solution annealing
AG	700 + 540	1 h + 8 h	Air	Peak aging[18]
R800-60m	800	1 h	Ar	Ref. [15]
N800-90m	800	1.5 h	Ar	New treatment
N800-180m	800	3 h	Ar	New treatment
P470-5m	470	5 min	Air	Post-deformation (new)

m in the sample name equals minutes.

equipped with the X'celerator array detector. The Cu Kα radiation was directed along the longitudinal direction of the polished samples. The accelerating voltage was 40 kV and the current was 30 mA. The scan was obtained for the range 30°2θ–90°2θ, with a step size of 0.0017°2θ and counting time of 80.010 s per step. XRD analysis was conducted using MAUD (MAUD 2.94; Luca Lutterotti[20]).

RESULTS

Quasi-Static Mechanical Behavior

Compared to the standardized peak-aging (AG) condition, both Young's modulus and flow stresses decrease when the material is quenched from 800° C, above transus (Fig. 2a).

Extended annealing durations further reduced the yield stress (σ_y) and plateau stress values (Table II). This is consistent with a Hall–Petch
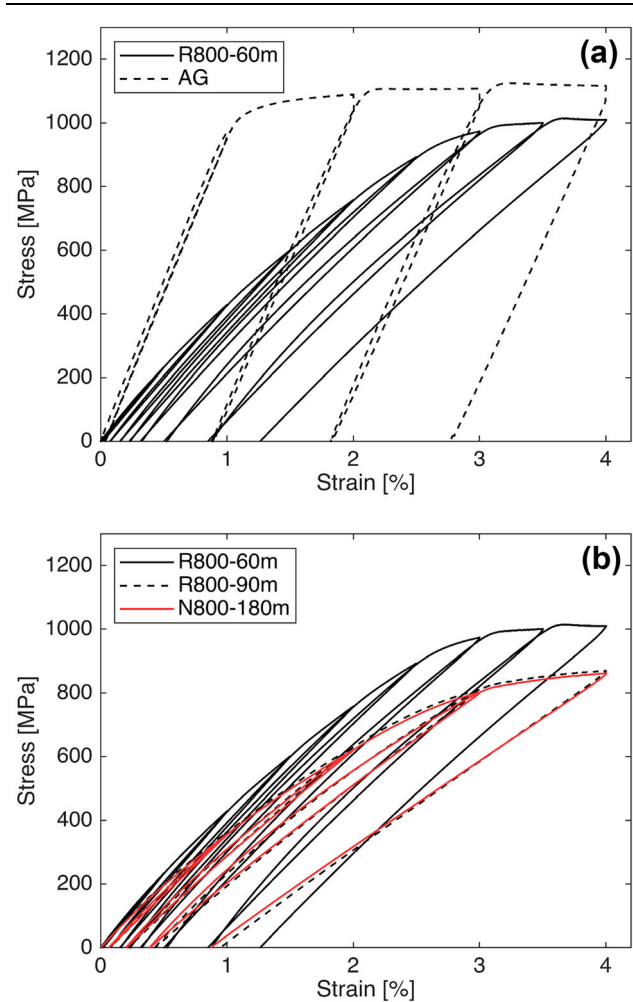
Fig. 2. Effects of heat treatments alone (no plastic pre-deformation) on tensile stress–strain characteristics (loading–unloading cycles, incremental maximum strain). Comparisons between (a) AG and R800-60m, and (b) R800-60m, R800-90m, and N800-180m

behavior (cf. section "Results of metallographic analysis").

It is also observed that larger plastic deformations corresponded to higher σ_y, but to lower values of Young's modulus E. Interestingly, upon application of a stress-relieving post-treatment (P470-5m) after the plastic deformation, the low-strain part of the curve straightens and E revert to higher values (Fig. 3a).

Some residual strains caused by plasticity are observed for all the samples at the end of each cycle, but were found to be reduced for heat treatments of longer durations (90 min or 180 min vs. 60 min; cf. Fig. 2).

Looking at the hysteresis loop amplitude (a measure of energy dissipation), the investigated samples are characterized by a common strain-dependent behavior, which yields similar results within each one of three distinct ranges, identified according to the maximum strain amplitude reached in the cycle: a low range from 0% to 0.5%, an intermediate one from 1% to 2%, and a high one from 2.5% to 3.5% maximum strain amplitudes. The hysteresis areas grow as the maximum strains increase, especially for cycles in the intermediate–high strain ranges. The results, in terms of hysteresis loop area as a function of the strain amplitude, for R800-60m and N800-180m subjected to different pre-deformations, are shown in Fig. 4. Comparable results are obtained, for both treatment durations, at strains below 1%. For larger strain amplitude values, however, a net increment in loop area between the undeformed and deformed samples is observed. The highest values of dissipated energy, on average, are obtained with a 16% pre-deformation.

Higher annealing times (e.g., N800-180m) yield, on average, a higher damping capacity if compared to the reference R800-60m. Best-performing conditions, especially for high ranges of strains, are achieved with a large pre-deformation value (16%). A comparison among the as-received, aged, standard, and damping-optimized samples is shown in Fig. 5, in which it can be seen that thermo-mechanical processing has a profound effect on the ability of the material to dissipate energy in mechanical cycles: for medium–high strains, the alloys subjected to the new processes outperform in this respect the material in its pristine and aged conditions.

The effect is even more remarkable for larger strains (4%), where the area of the hysteresis is more than doubled (N800-180m+16% vs. AG; cf. Figure 5) and a lower residual strain (Fig. 3b) is achieved when compared to the aged sample (Fig. 2). This much improved ability to recover strains is likely due to a change in deformation mechanisms, with a reduced slip component and an increase in partially reversible mechanisms (see Discussion).

Table II. Young's modulus E and yield stress σ_y for different thermo-mechanical treatments

Sample	σ_y (σ_m) (MPa)	E (GPa)	Sample	σ_y (σ_m) (MPa)	E (GPa)
R800-60m+9%	1039 (984)	45.6	N800-180m+9%	920 (885)	45.6
R800-60m+12%	−(984.4)	39.6	N800-180m+12%	928 (903)	39.6
R800-60m+16%	−(998)	36.2	N800-180m+16%	−(911)	36.2

The symbol "−" appears if σ_y could not be evaluated due to the lack of a clear yield point. The stress value σ_m, given in parentheses, is calculated on the plastic plateau at the maximum strain.
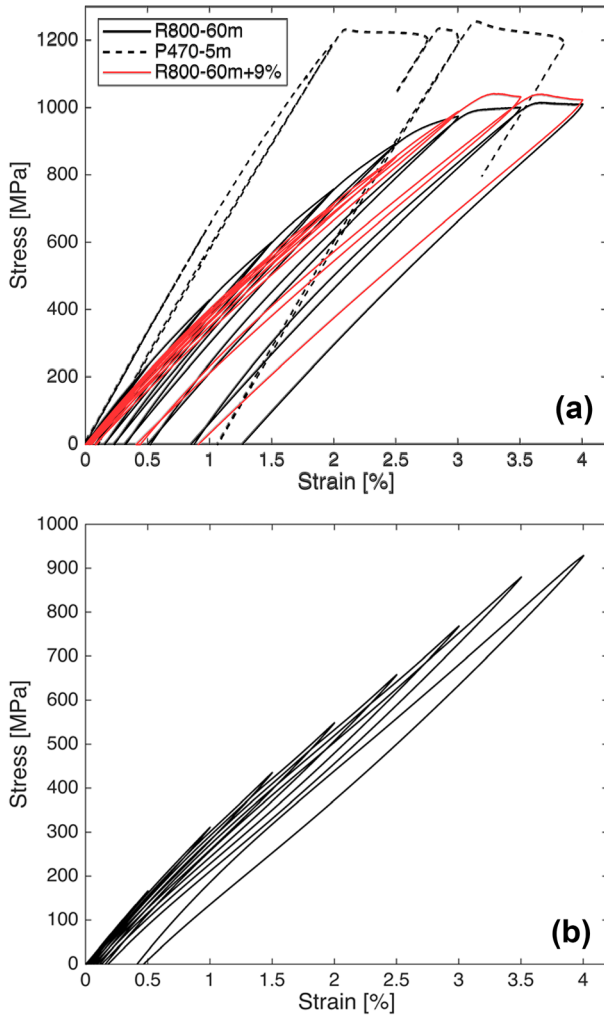
Fig. 3. A Effects of post-treatments on R800-60m+9%: stress–strain behavior after plastic deformation (red) and with further stress-relieving P470-5m (dashed black), compared with R800-60m (black). B Stress–strain curves of N800-180m after plastic deformation to 16% strains. Loading–unloading to incremental maximum strains. Notice increasing hysteresis area for increasing maximum strains, and generally limited residual strains upon unloading (Color figure online).

Dynamic Mechanical Characteristics

The dynamic response of the aged material (which underwent failure for a strain amplitude of 2.5%) is
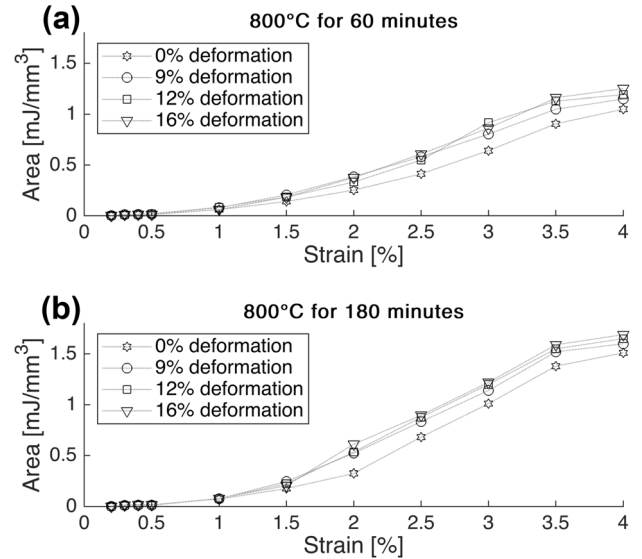

Fig. 4. Hysteresis areas for incremental maximum strains: comparisons between R800-60m (A) and N800-180m (B), for different values of pre-applied plastic deformation.

characterized by a lower damping capacity when compared to samples subjected to the new thermomechanical treatments.

The material aged at 800°C displays both amplitude-dependent and frequency-dependent behaviors.

As for the static case, it is useful to identify three different ranges of applied strain amplitudes: 0–1%, 1–2%, and 2–4%, as the material behavior seems to change from one range to the next.

Lower values of tanδ are obtained in the low-amplitude range if compared to the intermediate and high ones, which are nearly overlapped, for the samples treated at 60 min and 90 min (Fig. 5).

With N800-180m, however, the difference among the curves becomes less pronounced and the average value of tanδ, overall increases. Furthermore, a preferential strain amplitude condition is defined since, for a range of 1–2% of strain, a higher damping capacity is observed. Longer-lasting thermal treatments, on average, increase the tanδ for low amplitudes to values comparable with those obtained at shorter treatments for medium–high amplitudes.
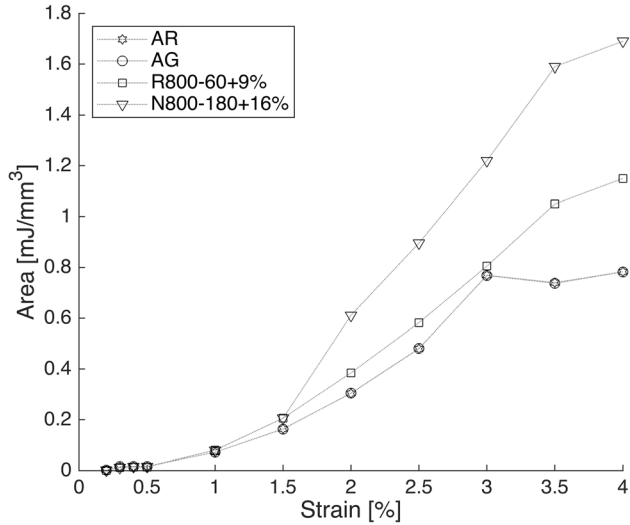
Fig. 5. Hysteresis areas for incremental maximum strains: comparisons between some different thermo-mechanical treatments: as-received, aged (*AG*), R800-60m+9% and N800-180m+16%.

Progressively larger values of plastic pre-deformation (9%, 12%, and 16%) increase, on average, the values of tanδ for both R800-60m and N800-180m. For a value of pre-deformation of 12% only, a possible extra peak is observed at 5 Hz.

Considering the frequency-dependent behavior, there is a background trend such that tanδ steadily decreases for increasing frequency in the 0 Hz to −20 Hz range. However, two noteworthy peaks are observed for R800-60m, N800-90m, and N800-180m, indicating resonant frequency conditions, at 10 Hz and 15 Hz (Figs. 6, 7).

In Fig. 7, bottom, the differences in damping obtainable with the peak ageing (AG), reference (R800-60m+9%) and optimized process (N800-180m+16%) can be appreciated.

Microstructure and Phase Composition

In the as-received state, the material is characterized by equiaxial β-phase grains (average size: 7.07 μm) with ω-phase precipitates at the boundaries, likely the result of quenching during the production of the material.[19] The presence of the secondary phase was revealed by SEM with backscattered electron contrast, supported by energy-dispersive X-ray analysis of darker areas of the sample (found to be Mo-lean), and later confirmed by XRD. Aging treatment (AG) promoted the intragranular nucleation of the Widmanstätten α-phase, as confirmed by the increased α-phase reflections in XRD (Fig. 8), and the cross-polarized metallography with oxalic tint (Fig. 9). The formation of the secondary phases is also in agreement with the observed TG-DTA peaks.

Annealing at 800°C had the effect of increasing the grain size, up to 22.56 μm for 1 h and to 33.18 μm for 3 h, while no statistical difference was recognized between 90 min and 180 min of treatment (Table III).

Simultaneously, a stabilizing effect on the β-phase, as witnessed by the progressive disappearance of secondary-phase related peaks, is obtained for prolonged treatment times. RD peaks are shifted from the ideal position, have a broadened profile after mechanical deformation, and present an additional asymmetric broadening of the base (Fig. 10a, b). Since this feature is often reported for high-symmetry crystals in conjunction with the
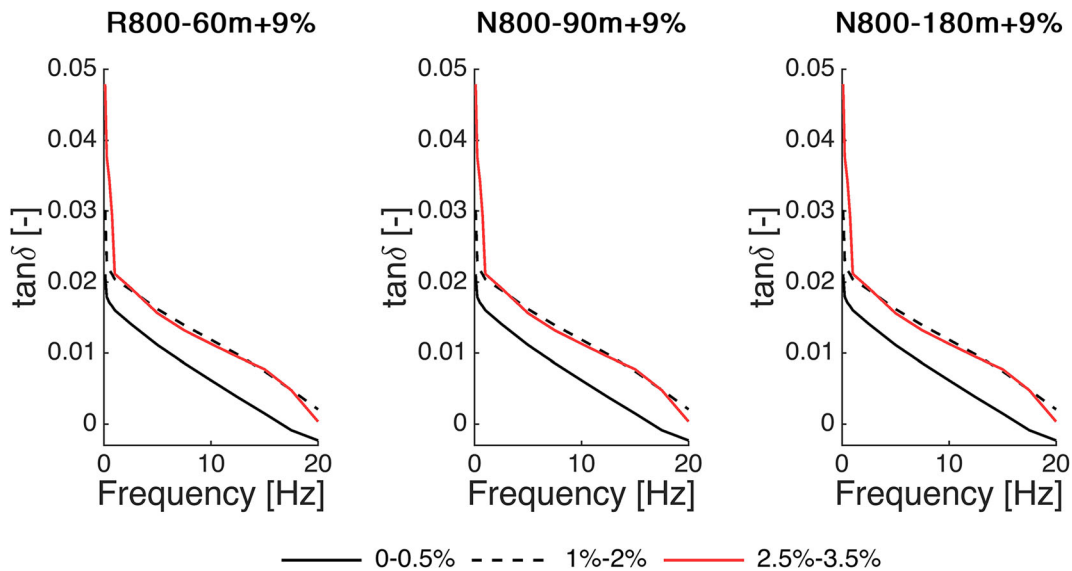

Fig. 6. Variations in tanδ according to frequency and strain amplitude for R800-60m (left), N800-90m (center) and N800-180m (right), all deformed up to 9%
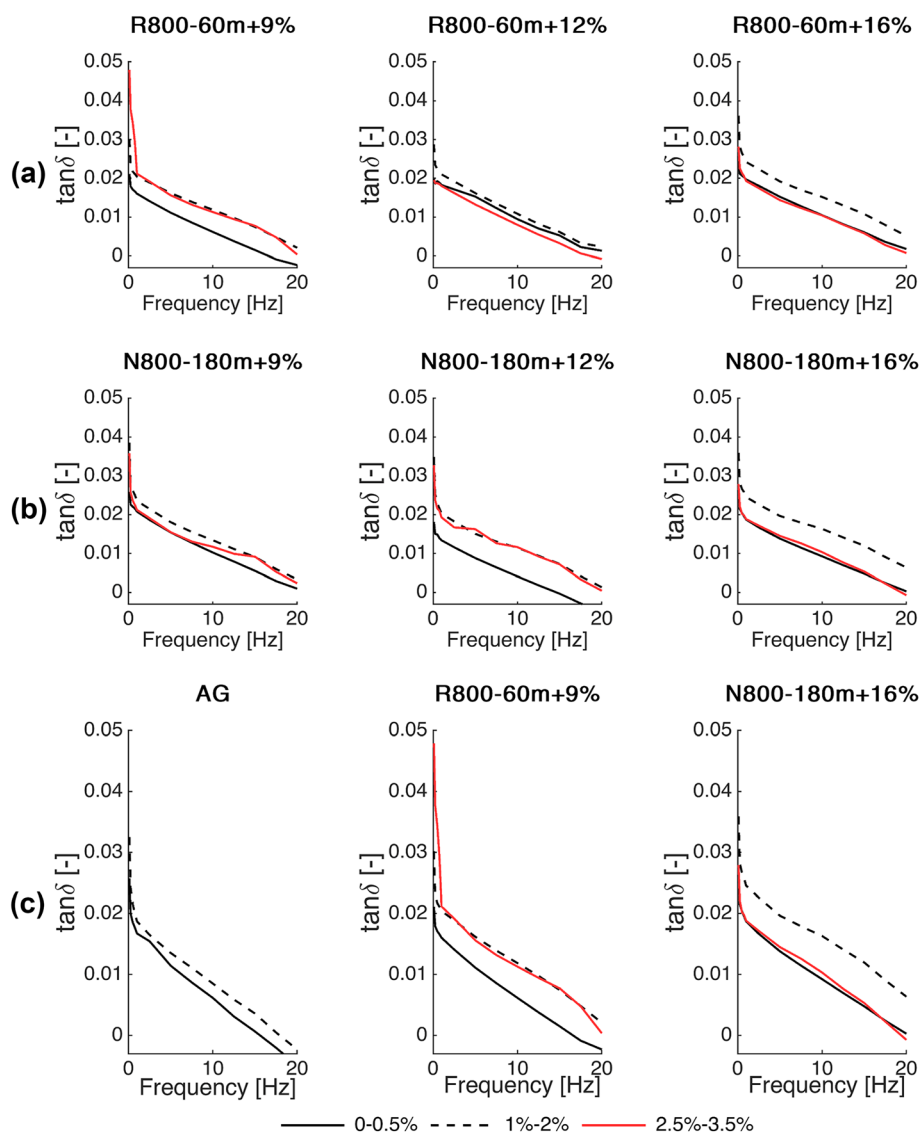
Fig. 7. Values of tanδ as a function of frequency samples R800-60m (a) and N800-180m (b). The effects of pre-deformation (9%, 12%, and 16%) are compared in the panels. Comparison of damping for the peak-aged (*AG*), reference (R800-60m+9%) and optimized (N800-180m+16%) process (c).

presence of stacking faults and twin boundaries, optical microscopy was employed to determine the state of the material after deformation.

Bright-field imaging revealed intra-grain plate-like structures, which taper near the boundaries, a typical feature of mechanical twins, while the use of cross-polarized illumination did not reveal stress-induced martensite (Fig. 9c), whose peaks were correspondingly not observed in the X-ray diffractograms (Fig. 10c, d).

DISCUSSION

Relationship Between Thermo-mechanical Treatment and Mechanical Characteristics

With respect to the as-received condition, the standard ageing treatment (AG) increases both the elastic modulus (98.68 GPa vs. 62.5 GPa) and yield stress (991.2 MPa vs. 958.9 MPa), while the reference heat treatment (R800-60m) results in controlled grain growth and reduced yield stress, and, when followed by mechanical deformation, appears to enhance the damping capacity of the alloy.

The newly presented heat treatments with longer annealing times determined a further reduction in yield stress due to the increased grain size, in accordance with the Hall–Petch relationship. Progressively larger mechanical pre-deformation values not only produced a strain-hardening effect but also a softening in primary stiffness. This peculiar behavior may be explained by the intervention of a secondary deformation mechanism with lower activation energy than slip, competing with the purely elastic one. The emergence and amplification of this new mechanism appears to be related to the presence of residual plastic pre-strains: a secondary heat
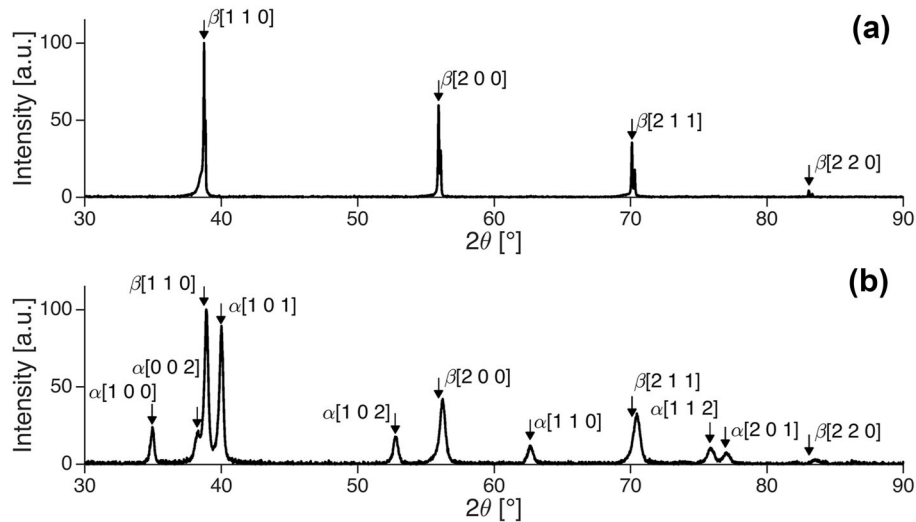
Fig. 8. X-ray diffraction profile of Beta III titanium alloy, as-received (a), and aged (b).
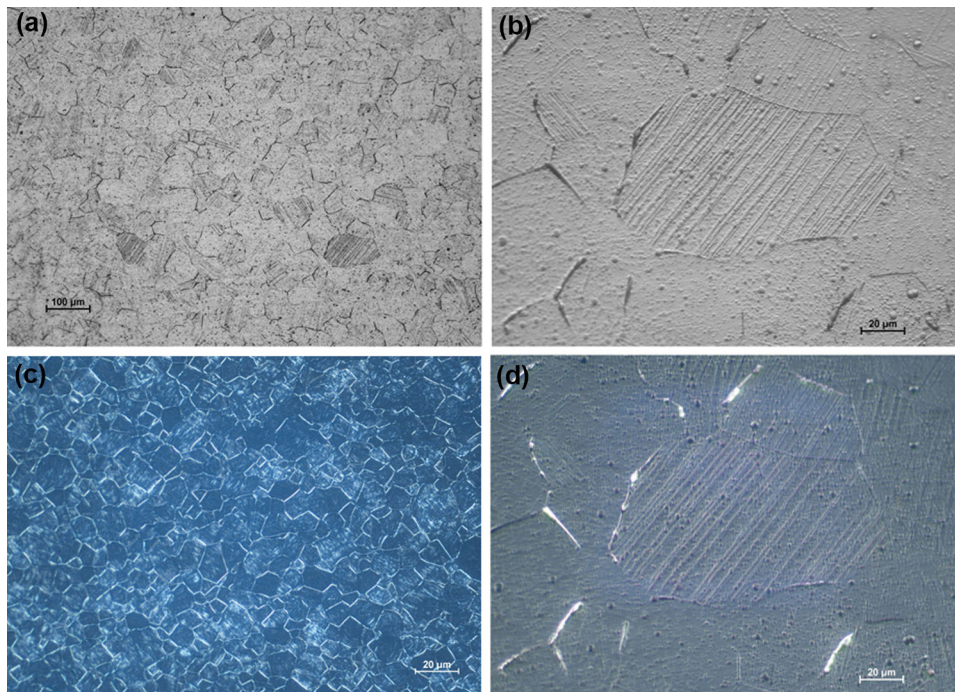

Fig. 9. Bright-field (a, ×10; b, ×50) and cross-polarized illumination (d, ×50) micrographs of N800-180m+9% showing the presence of mechanical twins; etched with Kroll's reagent. c, Cross-polarized illumination micrograph (×50, etched with oxalic tint) of the aged (*AG*) sample. Widmanstätten α-phase precipitates appear brighter in the middle of the grains.

treatment (70 GPa with P470-5m, applied to produce recovery, and whose short duration was specifically chosen to avoid any secondary phase precipitation, confirmed that stress relieving is able to cause reversal of this effect with a restoration of a higher elastic modulus).

The same thermo-mechanical processing also enhances the ability of the material to dissipate energy with respect to either as-received or aged state. Indeed, for medium–high amplitude strains (1.5–4%), we no-

ticed that progressively larger hysteresis areas were created for heavily deformed samples. As a matter of fact, the sample N800-180m+16% combines, for high-amplitude strains (4%), an improved hysteresis (more than twice the aged sample), a smaller residual strain (0.4% vs. 1.5%) with a contained reduction in yield stress (911 MPa vs. 991 MPa).

Considering the deformation mechanisms of the Beta III alloy, as predictable by the Kuroda chart, the most likely phenomena giving rise to modulus

Table III. Summary of the average grain sizes according to the thermo-mechanical processing

Sample	Grain size (μm)	Sample	Grain size (μm)
Heat treatments only			
AR	7.07	R800-60m	22.56
AG	6.72	N800-90m	31.62
		N800-180m	33.18
Heat treatment followed by plastic deformation			
R800-60m+9%	24.61	N800-180m+9%	33.60
R800-60m 12%	23.80	N800-180m 12%	34.00
R800-60m+16%	23.97	N800-180m+16%	32.87
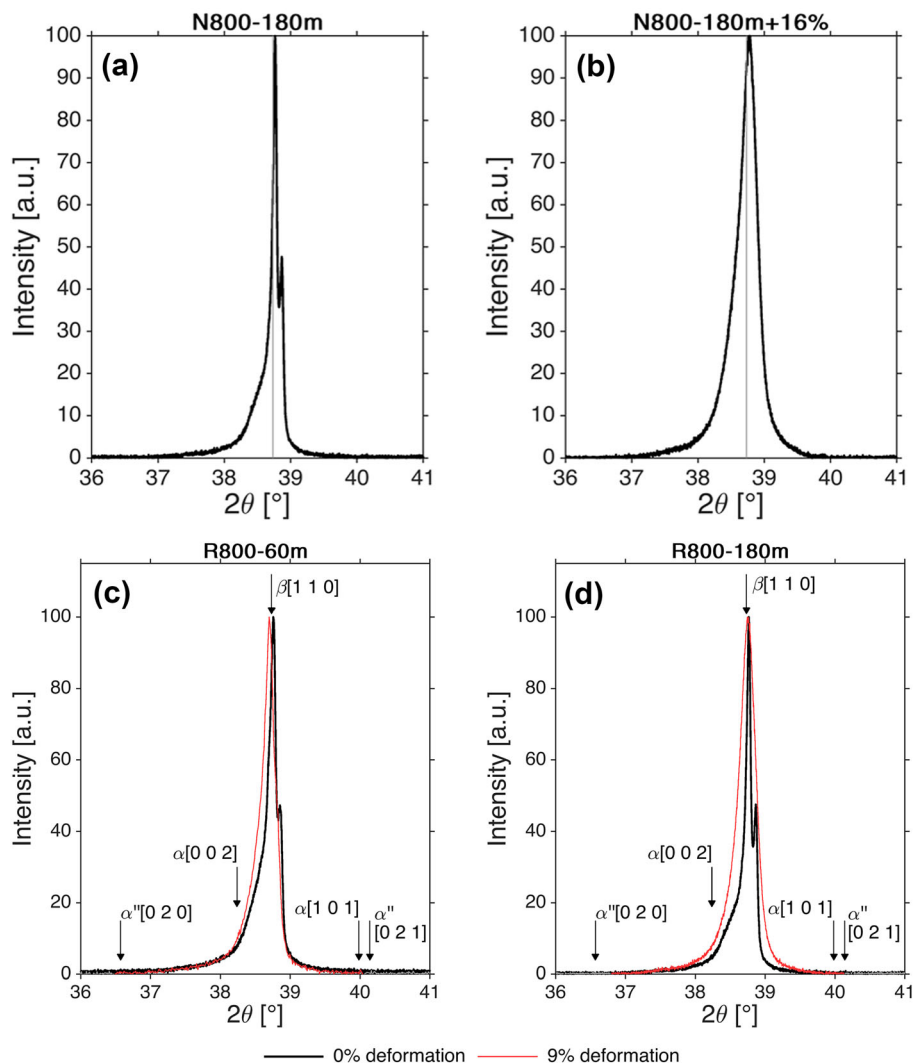
Fig. 10. XRD spectra in the 36°–41°2θ range for N800-180m, as-heat-treated (a) and plastic deformation to 16% strains (b). No peaks corresponding to the α''-phase are visible. The position of the β-phase peak is highlighted in gray. XRD spectra in the 36°–41°2θ range for R800-60m (c) and N800-180m (d), as-heat-treated, and with plastic deformation to 9% strains. No peaks corresponding to the α''-phase are visible in any case.

softening and development of the hysteresis, involve twinning or the formation of a thermoelastic α''-martensite. In either case, we should consider a mechanism with a reversible character, since we observed a reduced plastic deformation even when applying strains up to 4%.

Microstructural Correlations

Twins were observed in the samples heat-treated at 800°C, especially for extended durations, and then exposed to plastic deformation. In those samples, the larger grain size and the absence of secondary phases could be concurrent in creating the

basic conditions for a broader development of twins in the β-phase.

Twinning is often an irreversible phenomenon, so that a direct explanation of the large strain recovery observed in the cyclic loading tests by this mechanism alone is unlikely. On the other hand, we think that the residual stresses introduced with plastic deformation could produce elastic spring-back action at the twin boundaries, enabling a partial reset of the twinning induced upon loading. In the literature, the effect is referred to by the name of "elastic twinning."[21–23] The driving force for detwinning is related to the coupled effect of compatibility stresses in the twinned microstructure (which can be of the same order of magnitude as externally applied stresses) and stresses generated by dislocation loops at the partially incoherent twin/matrix interfaces. Energy dissipation by friction[21] would thus occur during the forward and reverse motion of these structures when cyclic external strains are applied. This reasoning is coherent with the observed disappearance of the hysteresis when a stress recovery heat treatment (P470-5m) is carried out after plastic deformation.

Another possible explanation, which takes into account the results of the previous works outlined in the Introduction,[15,16] would include the formation of a certain amount of stress-induced α"-martensite. The composition of our material batch corresponds to $\overline{B_o}$ and $\overline{M_d}$ values closer to the SIM zone than the nominal Beta III. In spite of this, no α"-phase is visible in our samples (which we always and only observed in externally-unloaded conditions), so we should conclude that, if some α"-phase is formed during the loading steps, it must then completely disappear upon unloading. The partial recovery of twinning of our first proposed mechanism could then be seen as a pre-martensitic phenomenon characterized mostly by the shearing, but lacking the Bain distortion.

In the scientific community, the mechanisms of formation and reduction of twins, in particular {332} <113> (that, incidentally, were confirmed for the first time by Blackburn and Feeny in Beta III alloy[24]) is still a matter of debate,[25,26] especially for non-superelastic β-Ti alloys.

There are two main theories: shear-shuffle[27] and α"-assisted. The first one, which does not include the formation of a martensite, admits direct nucleation from the β-phase, while the second presupposes that the twins originate upon reversal of a primary α"-phase. Recent results show that either mechanisms are possible, for instance for different deformation energy conditions.[26]

The micromechanical models that we hypothesized to explain the results of our experimental tests will need to be proven. Their validation is left for future work.

Dynamic Behavior

The DMA results showed that different thermomechanical histories affect the damping capacity of Beta III. Longer annealing times correspond, on average, to higher tanδ values. On the other hand, the dependency on the amplitude is not monotonic but has in fact a maximum in the intermediate range.

These observations point to the fact that the mechanism by which the quasi-static hysteresis is expanded by larger strain amplitudes may be related to, but different from, the one underlying the rise in tanδ. Clearly, both phenomena depend on dislocation density and probably on related pinning stresses. While the static one, as discussed in the previous section, may be explained by a pinning-unpinning of the twin boundary, the dynamic behavior could depend on the motion of the dislocations themselves constrained by the presence of other defects, as is often the case in cold-worked body-centered cubic metals and Titanium, where the increased interaction of these defects is known to enhance strain-independent (frequency-dependent) internal friction.[28]

Upon increasing of the concentration of deformation microstructures, like dislocations and twins, one observes a spreading of dissipation mechanisms across all frequencies (related to different local environments) and may assume that the (quasi-) reversible motion of the defects is limited to a distance beyond which they become irreversibly displaced (slip). Apart from these frequency-independent effects, it appears that in all conditions the samples display two peaks, indicating resonant frequency conditions, at 10 Hz and 15 Hz, whose origin has not been investigated in this work. How much such peaks dominate the spectrum actually seems to depend on the height of the background, as previously discussed.

Applicability

The observations made through static and dynamic mechanical testing confirmed that thermomechanical processing has a significant impact on the ability of the alloy to effectively damp oscillations, as the hysteresis can be increased, as well as the tanδ, across the frequencies of interest (0–20 Hz). Also, maximum dissipation is achieved in an intermediate strain amplitude range such as 1–2%.

The remarkable improvement in damping capacity of this alloy obtained with the N800-180m+16% process could be a noteworthy result in the aerospace field: different studies[29,30] have demonstrated the presence of characteristic helicopter vibration peaks at, respectively, 5 Hz and 10 Hz. The prolonged exposure to cyclic compressive forces can increase the load imposed on the spines of the pilots during flight, with consequent cases of back pain and spinal injuries.

The combination of a reduced elastic stiffness and improved damping capacity in the 0–20 Hz range of frequencies (typical, for example, of gait or physical activity-related musculoskeletal loading, and neurological disorders like tremor and dyskinesia) may also be interesting for the fields of sports and rehabilitation devices, including the design of wearables, orthotics, and prosthetics. Low moduli and controlled viscoelastic characteristics can provide improved biomechanical compatibility with the human body.

During the dynamic characterization, the damping-optimized wires have been subjected to a remarkable number of stress cycles (more than 10^4 cycles), proving their oligo-cyclic reliability. Fatigue life in the millions of cycles and definite frequency ranges is certainly a crucial structural property worth of further study in future.

CONCLUSION

Beta III metastable β-Ti alloy has been studied in order to evaluate how supertransus annealing followed by plastic deformation affects its mechanical properties, in particular damping.

The best results in terms of energy dissipation capacity were obtained with a heat treatment at 800°C for 3 h followed by plastic deformation to 16%. When compared to a standard (peak) aging treatment, the material displays an improved damping capacity both in quasi-static (on average, a 75.55% hysteresis increase for a strain amplitude higher than 1.5%) and dynamic conditions (on average, a 211.55% increase in tanδ across all the analyzed frequencies). The proposed process entails a concurrent reduction in Young's modulus (36.2 GPa vs. 98.68 GPa) and yield stress (911 MPa vs. 991.2 MPa) relative to the peak-aged sample, which constitutes the trade-off between maximizing just stiffness and strength or also damping.

The micromechanical phenomena underlying the increase in damping capacity of the Beta III alloy with the proposed treatment appear to be connected with the reversible motion of semi-constrained structures, namely twin boundaries interacting with dislocations. Our set of experiments could not confirm the involvement of martensitic transformations, or the α''-phase.

ACKNOWLEDGEMENTS

FUNDING

DATA AVAILABILITY

The raw/processed data required to reproduce these findings cannot be shared at this time due to technical or time limitations.

CONFLICT OF INTEREST

The authors declare that they have no conflict of interest.

OPEN ACCESS

REFERENCES

1. G. Lütjering and J.C. Williams, *Titanium*, *II* (2007).
2. S. Gialanella and A. Malandruccolo, Aerospace alloys, *Book*, pp. 480–492 (2020).
3. L.Y. Chen, Y.W. Cui, and L.C. Zhang, *Metals* 10(9), 1–29 https://doi.org/10.3390/met10091139 (2020).
4. R.P. Kolli and A. Devaraj, *Metals*. https://doi.org/10.3390/met8070506 (2018).
5. K. Endoh, M. Tahara, T. Inamura, and H. Hosoda, *Mater. Sci. Eng. A* 704, 72–76 https://doi.org/10.1016/j.msea.2017.07.097 (2017).
6. Y.K. Favstov and Y.A. Samoilov, *Met. Sci. Heat Treat.* 25(9), 679–681 https://doi.org/10.1007/BF00707287 (1983).
7. T. Inamura, H. Hosoda, K. Wakashima, J. Il Kim, H.Y. Kim, and S. Miyazaki, *Mater. Trans.* 48(3), 395–399 https://doi.org/10.2320/matertrans.48.395 (2007).
8. F. Yin, L. Yu, D. Ping, and S. Iwasaki, *Mater. Sci. Forum* 614, 175–180 https://doi.org/10.4028/www.scientific.net/MSF.614.175 (2009).
9. F. Yin, L. Yu, and D. Ping, *Mater. Sci. Eng. A* 521–522, 372–375 https://doi.org/10.1016/j.msea.2008.09.090 (2009).
10. I.G. Ritchie and Z.L. Pan, *Metall. Trans. A* 22, 607–616 (1991).
11. D. Kuroda, M. Niinomi, M. Morinaga, Y. Kato, and T. Yashiro, *Mater. Sci. Eng. A* 243(1–2), 244–249 https://doi.org/10.1016/s0921-5093(97)00808-3 (1998).
12. M. Bignon, E. Bertrand, F. Tancret, and P.E.J. Rivera-Díaz-del-Castillo, *Materialia*. https://doi.org/10.1016/j.mtla.2019.100382 (2019).
13. R.P. Kolli, W.J. Joost, and S. Ankem, *JOM* 67(6), 1273–1280 https://doi.org/10.1007/s11837-015-1411-y (2015).
14. P. Laheurte, Etude Du Comportement Pseudo Élastique D'Un Alliage De Titane Beta Metastable, Arcs Orthodontiques, p. 797 (2003).
15. P. Laheurte, A. Eberhardt, and M.J. Philippe, *Mater. Sci. Eng. A* 396(1–2), 223–230 https://doi.org/10.1016/j.msea.2005.01.022 (2005).

16. S. Cai, M.R. Daymond, Y. Ren, D.M. Bailey, and L.E. Kay, *Mater. Sci. Eng. A* 562, 172–179 https://doi.org/10.1016/j.msea.2012.11.005 (2013).

17. S. Cai, D.M. Bailey, and L.E. Kay, *J. Mater. Eng. Perform.* 21(12), 2559–2565 https://doi.org/10.1007/s11665-012-0302-4 (2012).

18. E.C.G. Welsch and R. Boyer, *Materials Properties Handbook: Titanium Alloys - ASM International.* 1994.

19. G. Welsch, R. Boyer, and E.W. Collings, Eds., "Ti-11.5Mo-6Zr-4.5Sn (Beta III)," in *Materials properties handbook: titanium alloys*, Materials Park, OH: ASM International, 1994, pp. 767–796.

20. L. Lutterotti, *Nucl. Instrum. Methods Phys. Res. Sect. B Beam Interact. Mater. At.* 268(3–4), 334–340 https://doi.org/10.1016/j.nimb.2009.09.053 (2010).

21. A.M. Kosevich and V.S. Boĭko, *Sov. Phys. - Uspekhi* 14(3), 286–316 https://doi.org/10.1070/PU1971v014n03ABEH004704 (1971).

22. T. Furuhara, K. Kishimoto, and T. Maki, *Mater. Trans. JIM* 35(12), 843–850 https://doi.org/10.2320/matertrans1989.35.843 (1994).

23. S. Pfeiffer and M.F.X. Wagner, *Proc. R. Soc. Math. Phys. Eng. Sci.* https://doi.org/10.1098/rspa.2017.0330 (2017).

24. J. A. Blackburn and M.J. Feeny, Stress-Induced Transformations in Ti-Mo Alloys (1970).

25. P. Castany, T. Gloriant, F. Sun, and F. Prima, *Comptes Rendus Phys.* 19(8), 710–720 https://doi.org/10.1016/j.crhy.2018.10.004 (2018).

26. J. Sun and L. Chen, *Metals.* https://doi.org/10.3390/met8121075 (2018).

27. A.G. Crocker, *Acta Metall.* 10(2), 113–122 https://doi.org/10.1016/0001-6160(62)90056-1 (1962).

28. T. Yamane, G. Mima, and J. Ueda, *Trans. Jpn. Inst. Met.* 5(3), 185–192 https://doi.org/10.2320/matertrans1960.5.185 (1964).

29. C.G. De Oliveira and J. Nadal, *Aviat. Space Environ. Med.* 76(6), 576–580 (2005).

30. M. Aykan and M. Çelik, *Mech. Syst. Signal Process.* 23(3), 897–907 https://doi.org/10.1016/j.ymssp.2008.08.006 (2009).